Environmental Science
Water Research & Technology

ROYAL SOCIETY OF CHEMISTRY

PAPER

View Article Online
View Journal | View Issue

Cite this: *Environ. Sci.: Water Res. Technol.*, 2025, **11**, 2412

Efficient preparation of adsorption beds from polycarbonate and cotton fabric wastes: removal of nitroaromatic pollutants from water

Tomaszewski Waldemar, *[a] Krasiński Andrzej,[b] Zybert Magdalena,[a] Wieciński Piotr[a] and Gołofit Tomasz[a]

Received 18th July 2025,
Accepted 25th July 2025

DOI: 10.1039/d5ew00669d

rsc.li/es-water

The pollution of the environment with explosives and their decomposition products, particularly resulting from armed conflicts and intensive mining activities, poses a serious problem nowadays. In this work, the properties of a novel and environmentally neutral adsorbent were investigated, which was used further to remove nitroaromatic explosives from wastewater. The adsorbent was prepared in a straightforward way from waste raw materials by applying a composite of polycarbonate and fumed silica to cotton fabric. On both laboratory and bench scale (flow system with recirculation), a new bed demonstrated high efficiency for removal of nitroaromatics from water, exceeding 90% for trinitrotoluene (TNT). It was also confirmed that the bed is suitable for removing explosive substances from real river water. The sorption properties of the material were related to its characteristics obtained using spectroscopic, microscopic, and thermal analysis, nitrogen adsorption, and adsorption kinetics and isotherms.

Water impact

Explosives are classified as emerging contaminants in recent years. A novel adsorbent was prepared from waste polycarbonate and cotton fabric for the removal of nitro explosives from water. In laboratory and bench scale the adsorbent is characterized by high adsorption capacity.

1. Introduction

This study presents a novel approach for the simultaneous utilization of materials derived from two significant categories of anthropogenic waste – namely, waste textiles and waste plastics, specifically cotton fabric and polycarbonate – for the removal of hazardous environmental toxins, particularly nitroaromatic compounds, from aqueous solutions. The first section of the introduction provides a brief overview of the selected waste materials and the environmental risks associated with nitro compounds. These two issues are then brought together in the final part of the introduction, forming the conceptual basis of the paper.

Textile and plastics production constitute important sectors of the global economy, with millions of employees worldwide. The global production and disposal of textiles composed of both natural-origin materials and fibrillated polymers, along with a variety of plastic products exhibiting diverse morphologies, is constantly growing. This trend presents significant environmental and societal challenges. This requires a comprehensive global framework for the management, disposal, and environmental monitoring of such materials, particularly in natural systems such as aquatic environments, soils, and even the atmosphere, where fragmented forms, most notably microplastics, may accumulate and persist.

In 2022 the global textile production amounted to 116 million tons,[1] whereas the production of plastics is 400 million tons.[2]

Both production types experienced a significant growth compared to 2021. The two industries have been criticized for unsustainable use of water, land, fossil fuels and energy as well as production processes involving toxic chemicals, waste and pollution. Currently, millions of tons of waste such as used clothes and plastics raise a major concern as well, and therefore more attempts to recycle textiles[3] and plastics[4] are undertaken. Studies on the use of waste textiles and plastics to remove other environmental pollutants have been published. Fabric-based adsorbents have been used to

[a] *Faculty of Chemistry, Warsaw University of Technology, 3 Noakowskiego Street, 00-664 Warsaw, Poland. E-mail: waldemar.tomaszewski@pw.edu.pl*
[b] *Faculty of Chemical and Process Engineering, Warsaw University of Technology, Waryńskiego 1 Street, 00-645 Warsaw, Poland*

remove various pollutants from water, including pesticides,[5] heavy metals[6] and dyes.[7] There have also been attempts to use plastic waste to produce adsorbents that would eliminate heavy metals,[8] oil stains[9] and dyes[10] from water.

Nitroaromatic compounds represent a group of hazardous environmental pollutants that are neurotoxic and are possible human carcinogens.[11] Due to their high chemical stability and persistence, these compounds can remain in water and soil for extended periods of time.[12] This group of compounds primarily includes components of explosives that enter the environment as a result of military, mining, and armament production activities. In addition to such activities, these compounds are also used in chemical processing, for example, dinitrotoluenes are used in the production of polyurethanes.[13] Significant environmental contamination by nitrotoluenes also occurs as a result of armed conflicts (*e.g.*, in Syria, Ukraine, and Central Africa).[14]

Technologies for removing nitrotoluenes from the aquatic environment are primarily based on separation methods and degradation processes.[15] Among separation methods, adsorption is the most commonly used.[16] For the degradation of nitroaromatics, commonly employed methods include advanced oxidation processes (AOPs), such as the photo-Fenton process,[17] bioremediation,[18] and phytoremediation.[19]

Among these remediation techniques, adsorption on granular activated carbon (GAC) is most frequently applied for treating surface waters. This is due to the simplicity and effectiveness of the method. However, it comes with high costs related to GAC production, disposal of spent carbon, or its regeneration.[15] It should be noted that high-temperature carbon regeneration is not used due to safety risks when the explosive content in the matrix exceeds 8% by weight.[20] Other methods such as hydrolysis,[21] solvent extraction,[22] or heat steam-air treatment[23] are used for regenerating activated carbon loaded with explosives. However, the high energy and chemical consumption involved in these processes drive the search for more sustainable and cost-effective adsorbents for the removal of nitroaromatics from surface waters. Recent studies suggest that adsorbents derived from agricultural or industrial waste may offer promising and economical alternatives. For instance, activated carbon obtained from spent coffee grounds has been shown to have low production costs and allows for easy solvent regeneration after TNT adsorption.[24]

Another inspiration for the below study came from a paper published in 2018.[25] This work used thin film passive samplers prepared on various substrate materials, including cotton, coated by dip-coating in solutions of polymers based on 2,6-diphenylene oxide, such as Tenax TA or PPO. The prepared samplers demonstrated efficient adsorption capacity of nitroaromatic vapors of explosive substances. The above results, along with an earlier publication[26] on the adsorption of explosives on acrylic and aromatic polymers, inspired the idea of preparing polycarbonate-based adsorption media for the removal of nitroaromatic compounds from water. In line with the above, the authors of this study aimed to explore the use of post-consumer waste, specifically cotton fabric waste and offcuts of polycarbonate sheets, for the development of a novel sustainable[27] adsorbent. To date, no published studies have reported such a use of these waste materials.

2. Materials and methods

2.1. Waste raw materials and chemicals

The polycarbonate (PC) came from the waste from panels used by a local canopy manufacturer. The 5 mm thick, triangle-shaped waste (Fig. S1 in the SI) was cut into smaller pieces using a hand-held metal guillotine. The cotton substrate came from unused 140 g m^{-2} cotton fabric withdrawn from a military warehouse (Fig. S2). As a solvent waste tetrahydrofuran (THF) was used. Its source was an effluent from the analysis by size exclusion chromatography (SEC), originally being an unstabilized BHT solvent of chromatographic purity (Avantor, Poland). Silica gel, analyzed sorbent for flash chromatography (irregular 40–63 μm, 60 Å), was obtained from Baker (Poland), whereas Aerosil R 972 V was obtained from Evonik. Aerosil R 972 V is a densified hydrophobic fumed silica after being treated with dimethyldichlorosilane. Norit SX-2 activated carbon was obtained from Chempur (Poland). Acetonitrile for liquid chromatography and deionized water were used for high-performance liquid chromatography (HPLC) quantification of explosives, while 2,4,6-trinitrotoluene (TNT), 2,4-dinitrotoluene (2,4-DNT), 1,3,5-trinitrobenzene (TNB), 2-nitrotoluene (2-NT), 1-nitronaphthalene (1-NN), and 1,8-dinitronataphthalene (1,8-DNN) came from the Department of Chemistry, Warsaw University of Technology.

2.2. Preparation and properties of adsorption bed

2.2.1. Adsorption bed preparation. Adsorption beds were obtained by applying a solution of PC in THF, with or without silica, to both sides of the cotton fabric using a paint roller with cotton coating. After the bed composition had been optimized (see discussion, section 2.2.2.2.), a solution in 720 mL of THF with 23 g of PC and 25 g of silica or Aerosil was used to prepare the adsorption beds. A metal frame, to which a 28 cm × 58 cm fabric (Fig. S3) was attached, was placed under the ventilation hood. Each side of the central area of the 20 cm × 50 cm fabric was progressively and evenly covered with half of the solution, using transverse and longitudinal movements of the roller. A total of 10–11 such cycles were completed, and after application of the phase, THF needed some time to evaporate. The fabric was then removed from the frame and fixed again on the reverse side. The bed was left to dry overnight and then cut into the appropriate size (Fig. 1). The reference material, *i.e.* containing only PC, was prepared in a similar way. The beds prepared on cotton fabric (C) were marked as follows: reference PC/C, with silica PC/Si/C, and with Aerosil PC/Ae/C.

For differential scanning calorimetry (DSC) and scanning electron microscopy (SEM) measurements, the samples of the adsorption phase alone were prepared, *i.e.* the one not applied to the cotton, but poured to form thin layers in Petri dishes. In

Fig. 1 The prepared adsorption flakes.

the case of DSC, this was caused by the fact that the decomposition of the cotton begins at temperatures above 180 °C. For SEM, this step facilitated the measurements and, most importantly, allowed the observation of undamaged samples. The obtained samples were designated as PC/THF, PC/Si, and PC/Ae.

2.2.2. Bed characteristics

2.2.2.1. Efficient amount of phase on textile. In order to determine the mass of the applied phase, a central part, *i.e.* 20 cm × 50 cm, was cut out from each bed and weighed. The mass of the fabric, *i.e.* 14 g, was subtracted from the resulting weight.

2.2.2.2. Fourier-transform infrared spectroscopy (FTIR). FTIR measurements were performed to determine the extent of coverage of the fabric by the applied phase. FTIR spectra were collected on a Nicolet 6700 spectrometer (Thermo Scientific) using an ATR accessory. Thirty-two scans were taken at a resolution of 4 cm^{-1} each.

2.2.2.3. Raman spectroscopy. The Raman spectra of the prepared cotton beds were collected to determine the crystal/disordered structure of PC. For this purpose, the intensities of the bands obtained from the deconvoluted spectra in the 750–710 and 1275–1200 cm^{-1} regions were compared. The spectra were recorded using a Thermo Nicolet Almega XR Raman spectrometer (Thermo Electron). Excitation was achieved using a 532 nm laser. The deconvolution of the bands was carried out using Omnic software (Thermo Fisher v. 9.1).

2.2.2.4. Low-temperature nitrogen adsorption. N_2 physisorption was applied to determine the specific surface area and total pore volume of the studied materials. The experiments were conducted at −196 °C using an ASAP2020 instrument (Micromeritics Instrument). Before the measurements, each sample was subjected to a two-step degassing procedure in vacuum: at 90 °C for 1 h and then at 120 °C for 4 h. The obtained data were approximated using Brunauer–Emmett–Teller (BET) and Barret–Joyner–Halenda (BJH) isotherm models.

2.2.2.5. Scanning electron microscopy (SEM). Morphology and microstructure observation as well as chemical analysis were performed with the use of a field emission scanning electron microscope (Helios 5 PFIB, Thermo Scientific) equipped with a Xe plasma FIB column and an EDS spectrometer (Octane Elice, EDAX). Thin Au coating was deposited onto the samples in order to ensure the conductivity of the surface. SE signal was applied to observe the surface morphology of the material.

2.2.2.6. Differential scanning calorimetry (DSC). In order to compare the degree of crystallinity of the prepared adsorbents DSC studies were performed, using a DSC Q2000 differential scanning calorimeter (TA Instruments). Indium was used for calibration as a standard substance. Measurements were carried out in open pans at temperatures from −100 to 300 °C, with a constant temperature increase of 10 °C min^{-1} and nitrogen flow of 50 mL s^{-1}.

2.2.2.7. UV-vis spectrophotometry. UV-vis absorption spectra of real river water samples were recorded on an Evolution 60S spectrophotometer (Thermo Scientific) at room temperature. Redistilled water was used as a reference sample.

2.3. Bed adsorption

2.3.1. Laboratory scale. The adsorption (q_t) of nitroaromatic substances from aqueous solutions on the prepared beds was expressed as the amount of substance adsorbed after a fixed time (t) per mass unit of the used bed and was calculated according to the formula:

$$q_t = \frac{(C_0 - C_t)}{m} V \quad (1)$$

where q_t is the amount of substance adsorbed after time t (mg g^{-1}), C_0 is the initial concentration (mg L^{-1}), C_t is the concentration after time t (mg L^{-1}), and V – solution volume (L), m – bed mass (g).

The adsorption kinetics was examined on two scales: lab-scale (1 liter) and bench scale (16 liters). On the lab-scale, 1 liter of nitro compound solutions with a concentration of 25 mg L^{-1} in redistilled water was placed in a 2 liter beaker. Such high concentration levels were chosen to ensure the collection of accurate and reproducible analytical data also in the case when a high level of the analyte has been removed by the beds. An adsorption bed in the form of 60 pieces of flakes of 1 cm × 1 cm was added to the beaker. The solutions were mixed at room temperature using a mechanical turbine stirrer at 200 rpm. Samples were collected at different time intervals depending on the experimental stage and analyzed by HPLC as described below. Such an experimental setup for the lab scale was chosen based on preliminary studies performed for TNT, where the variable parameters involved the rotation of stirrer and ionic strength of the solutions. The rotation was changed in the range of 0–400 rpm, while the ionic strength was increased using the addition of NaCl, *i.e.* 1% and 5%.

On the other hand, the adsorption isotherms were determined for TNT only. This relates to the conclusions in the discussion below, namely that the adsorption kinetics of the investigated nitro compounds show great similarities. Experiments to determine TNT adsorption isotherms on PC/Si/C and PC/Ae/C beds were performed on a scale proportional to the kinetic experiments, *i.e.* a 30-times reduced scale. 33 mL of aqueous solutions with concentrations ranging from 0.25 to 25 mg L^{-1} and two flakes of the size 1 cm × 1 cm were added to 50 mL conical glass flasks with screw caps. The flasks were shaken at 26 °C, 36 °C, and 46 °C for 24 hours. The collected samples were analyzed by HPLC as described below (section 2.3.3.).

In order to determine the effect of the natural matrix on the sorption capacity of the Pc/Ae/C adsorbent, the experiments were carried out on a 1-litre scale using flowing water from the Pilica River near Białobrzegi town, central Poland. After sedimentation, the water was poured into 1-liter volumetric flasks and stored in a refrigerator. Before starting the experiments, the contents of the flasks were poured into 2-litre beakers, where 1 mL of acetonitrile containing 25 mg of the nitro compound was added. According to a previous work[28] the addition of acetonitrile eliminated the biological activity in the water (bacteria, fungi) and stabilized its properties. After mixing the solutions, the corresponding samples were taken. Then the experiments were carried out as in case of lab-scale, except that only 3 samples were taken from each beaker after 48 hours of the experiment. The samples were filtered through 0.45 μm PTFE filters. HPLC analyses served to determine the concentrations and calculate the bed adsorption values designated as q_{river} (river) for the investigated nitroaromatics.

2.3.2. Bench scale. Sorption experiments were carried out in the system, which can be operated continuously in a wide range of flow rates (high flexibility), and can be easily scaled up to a desired capacity. The presented results show the performance of water cleaning in a closed loop, in which the liquid was circulated from the tank through the column containing sorbent elements. The system layout is schematically shown on the process flow diagram in Fig. 2.

Around 16 liters of water solution of a pollutant was prepared and poured into the tank (1) before each experiment. The initial concentration was 25 mg L^{-1}. Then the circulation pump (2) (centrifugal, produced by Grundfos, model CRNE 1–3) was switched on and the process was initiated. The water was pumped from the tank (1) through a vertical glass column and returned to the feed tank. The flow rate was controlled using the mass flow meter (3) (manufactured by Endress + Hauser, model Promass 40E15) and manually adjusted using the diaphragm valve (4); a flow rate of 400 L h^{-1} was used in experiments. The water samples for analysis were collected every 15 minutes (first hour) and then every 30 minutes. During the experiment the pressure drop on the column was also monitored. The flow characteristics of the experimental system are shown in Fig. S4. The column ID was 15 cm, and the total length was 40 cm. The sorbent elements, 1000 flakes of 1 cm × 1 cm, were loosely packed on a perforated plate (5 mm holes, free area around 30%) made of polyethylene.

2.3.3. Quantification of nitroaromatics in solutions. The aqueous solutions of nitro compounds – samples before and after experiments – were analysed using high-performance liquid chromatography (HPLC) using an Agilent 1260 Infinity system with a UV DAD detector. The separation was carried out with mobile phase acetonitrile/water on a Supelcosil ABZ + column (150 mm × 4.6 mm) at 50 °C. HPLC-grade solvents were used. Aqueous samples were taken and analysed without any preparation.

2.3.4. Adsorption kinetics – analysis of data. Two kinetic equations were used to describe the mechanism of adsorption kinetic data: a pseudo-first-order and a pseudo-second-order equation. The pseudo-first order equation[29] has the following linear form:

$$\ln(q_e - q_t) = q_e \ln - \left(\frac{k_1}{2.303}\right) \quad (2)$$

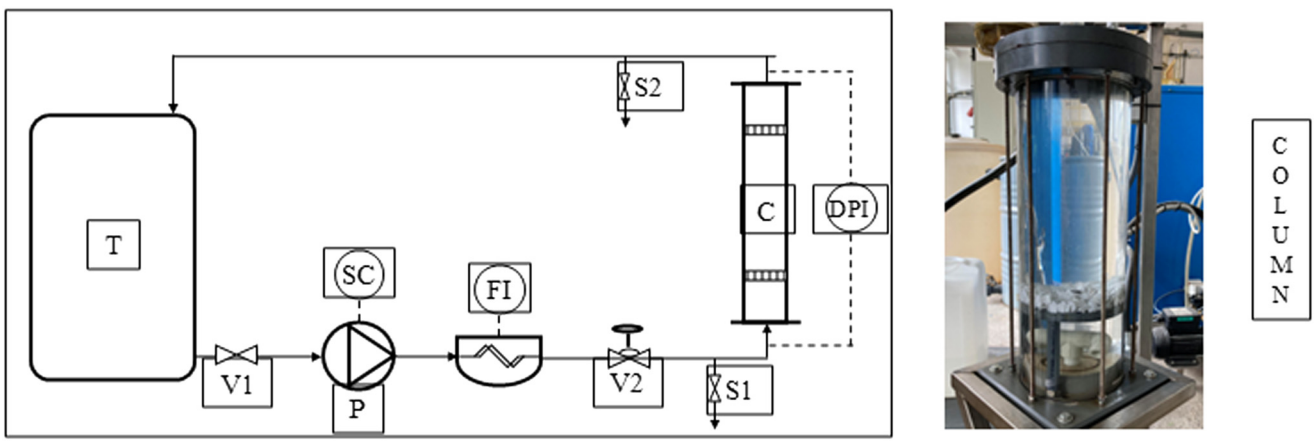

Fig. 2 Scheme of the experimental system (left) and photograph of the column (right): T, feed tank; V1, cutoff ball valve; V2, control diaphragm valve; S1 and S2, sample valves; P, circulating pump (with speed controller SC); FI, flow meter; DPI, differential pressure sensor; C, column.

where q_e is the amount of adsorption at equilibrium (mg g^{-1}), q_t is the amount of adsorption at time t (mg g^{-1}), k_1 is the first-order equation constant (1 min^{-1}), and t is the time (min).

The linear form of the pseudo-second-order equation[30] is as follows:

$$\frac{t}{q_t} = \frac{1}{k_2 q_e^2} + \frac{t}{q_e} \quad (3)$$

where q_t is the amounts of adsorption at time t (mg g^{-1}), q_e is the amount of adsorption at equilibrium (mg g^{-1}), k_2 is the second-order equation constant (g mg^{-1} min^{-1}), and t is the time (min).

2.3.5. Absorption isotherm – data analysis. Two adsorption isotherm equations were used to describe the adsorption of nitro compounds, namely Langmuir and Freundlich models.

The linear form of the Langmuir isotherm model[31] is as follows:

$$\frac{C_e}{q_e} = \frac{C_e}{q_m} + \frac{1}{K_L q_m} \quad (4)$$

where C_e is the concentration of solution at equilibrium (mg L^{-1}), q_e is the amount of adsorbed nitro compound at equilibrium (mg g^{-1}), q_m is the maximum adsorption capacity (mg g^{-1}), and K_L is the Langmuir constant (L mg^{-1}).

The linear form of the Freundlich isotherm equation[31] is as follows:

$$\log q_e = \left(\frac{1}{n}\right) \log C_e + \log K_F \quad (5)$$

where q_e is the amount of adsorbed nitro compound at equilibrium (mg g^{-1}), n is a constant, C_e is the concentration of solution at equilibrium (mg L^{-1}), and K_F is the Freundlich constant (mg g^{-1} $L^{1/n}$ $g^{-1/n}$).

2.3.6. Adsorption thermodynamics – data analysis. The thermodynamic parameters of adsorption, *i.e.*, free energy change (ΔG), change in enthalpy (ΔH), and change in entropy (ΔS), determine the spontaneity and feasibility of the adsorption process as well as the influence of temperature on its course. The determination of thermodynamic parameters is based on the van't Hoff equation, which is expressed as follows:

$$\ln K_{eq} = -\frac{\Delta H}{RT} + \frac{\Delta S}{R} \quad (6)$$

where R is the universal gas constant (8.314 J mol^{-1} K^{-1}), T is the temperature (K), and K_{eq} is the equilibrium constant. A plot of $\ln K_{eq}$ *versus* $1/T$ allows for the determination of ΔH (kJ mol^{-1}) and ΔS (J mol^{-1} K^{-1}) as the slope and intercept of the linear plot, respectively, multiplied by R.

The value of ΔG (kJ mol^{-1}) can be calculated using the equation:

$$\Delta G = -RT \ln K_{eq} = \Delta H - T\Delta S \quad (7)$$

For the non-ionic analyte studied, *e.g.* TNT (trinitrotoluene), the dimensionless equilibrium constant K_{eq} was obtained from the Langmuir constant K_L, according to Ghosal and Gupta,[32] by multiplying K_L by the molar mass of TNT expressed in mg mol^{-1} (227.13×10^3).

2.3.7. Solvent desorption studies. To investigate the desorption efficiency of TNT from PC/Ae/C, three samples of the sorbent with a known amount of deposited TNT were prepared. The samples were prepared in the same way as for the determination of adsorption isotherms. 33 mL of aqueous TNT solutions at a concentration of 25 mg L^{-1} and two flakes (1 cm × 1 cm in size) were placed in 50 mL conical glass flasks with screw caps. The flasks were shaken at 26 °C for 24 hours. After this time, the aqueous phases were collected and analyzed by HPLC. The equilibrium concentrations of TNT allowed the calculation of the amount of TNT adsorbed onto the sorbent.

The pre-adsorbed samples were subjected to extraction with acetonitrile (ACN). ACN was chosen because it is a good solvent for TNT and does not dissolve polycarbonate. Furthermore, the resulting extract can be directly analyzed by the applied HPLC method, unlike, for example, an acetone extract, which must be evaporated to dryness and then reconstituted before analysis. The desorption of TNT was carried out as follows. After the experiments, the sorbent samples were rinsed with water and dried on filter paper. Desorption was performed in 4 mL screw-cap vials containing two pieces of the sorbent, 2 mL of ACN, and a magnetic stir bar. The extraction was conducted for 15 minutes. Prior to analysis, the extract was diluted 16.5-fold with water (the initial volume of the water sample was 33 mL).

3. Results and discussion

3.1. Adsorbent preparation

In the preparation of 10 consecutive beds, it was found that the application of an average of 36 ± 1 mg of PC/Aerosil adsorbent phase and 33 ± 1 mg of PC/silica adsorbent phase per 1 cm^2 of fabric was possible. These values should be understood as the total amount of adsorbent present on both sides of the fabric. It should be recalled that based on the bed preparation conditions the maximum coverage could be 48 mg per 1 cm^2.

3.2. FTIR spectroscopy

Fig. 3 shows the spectra of reagents used to prepare the beds, as seen from top to bottom: Aerosil (A), cotton fabric (B), polycarbonate (C), fabric of coverage of 30 mg cm^{-2} of the PC + Aerosil mixture (D) and of 36 mg cm^{-2} coverage (E). The most intense observed vibrations are discussed below. For Aerosil the peak at 1100 cm^{-1} (1) can be attributed to asymmetric stretching vibrations of the Si–O–Si bonds and the peak at 820 cm^{-1} (2) can be assigned to the symmetric deformation vibration of the Si–O–Si bonds. For cotton fabric, the broad band at 3300 cm^{-1} (3) represents O–H stretching vibration and at 1030 cm^{-1} (4) C–O stretching vibration. For polycarbonate the characteristic peaks can be assigned as follows: at 1770 cm^{-1} (5), C═O stretching vibration; 1500 cm^{-1} (6), aromatic C–C stretching; and at 1230–1200 cm^{-1} (6), three peaks for O–C–O asymmetric

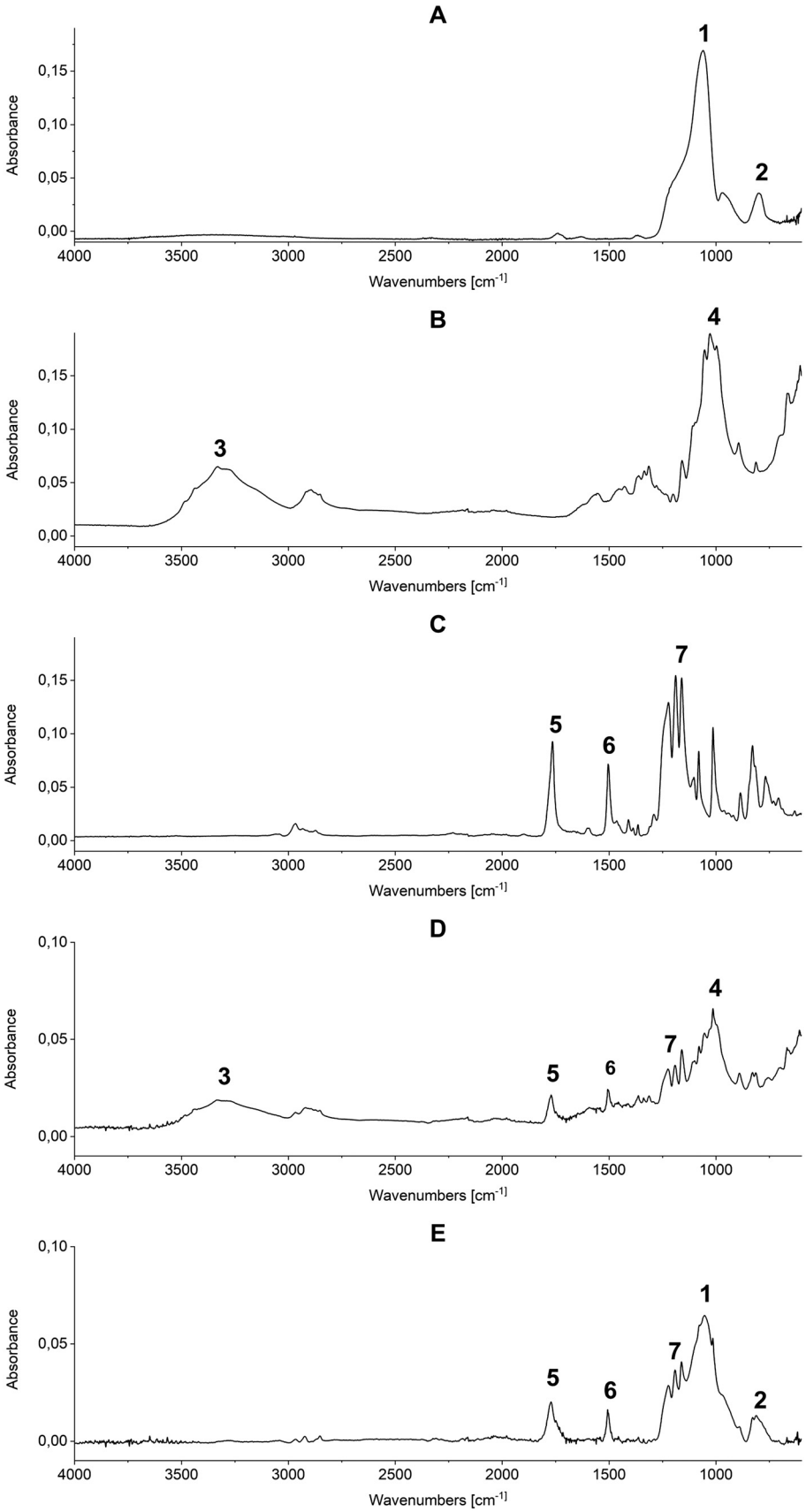

Fig. 3 FTIR spectra of prepared adsorbents. Optimization of cotton coverage with adsorption phase. The spectra are Aerosil (A), cotton fabric (B), polycarbonate (C), bed with planned coverage of 30 mg cm^{-2} PC/Aerosil (D) and with coverage of 36 mg cm^{-2} PC/Aerosil (E). Description of marked bands, see section 3.2.

Table 1 The intensity ratio of the bands representing ordered (727 cm^{-1}, 1248 cm^{-1}) and disordered (735 cm^{-1}, 1235 cm^{-1}) states of the adsorbents, obtained by the deconvolution of samples' Raman spectra

Sample	Intensity ratio I_{727}/I_{735}	Intensity ratio I_{1248}/I_{1235}
Initial PC	0.32	1.03
PC/cotton	0.84	1.05
PC/silica/cotton/	1.20	1.17
PC/Aerosil/cotton	1.24	1.26

stretching. The spectrum of cotton with a coverage of 30 mg cm^{-2} of the PC/Aerosil mixture is still characterized by O–H and C–O vibrations in cotton and PC vibration is also clearly visible. The broad bands of low specificity for silica are not represented. The O–H (3) and C–O (4) vibrations are no longer visible on the spectrum of cotton with a coverage of 36 mg cm^{-2}, while the broad bands attributed to Aerosil (1 and 2) can be observed. In comparison to the spectrum above (D in Fig. 3), the intensity of the bands attributed to PC is higher. Therefore, for the coverage of cotton with the phase at the value of 36 mg cm^{-2}, it was considered that the surface is completely covered by the adsorbent.

3.3. Raman spectroscopy

Raman spectroscopy was previously reported as a useful tool for analysis of the crystal structures of PC.[33] In accordance with this work the degree of the ordered structure of PC can be estimated from the intensity ratio of the peak at 727 cm^{-1} (order band) and 735 cm^{-1} (disorder band), and also the intensity ratio of the peak at 1248 cm^{-1} (order band) and 1235 cm^{-1} (disorder band). In short, the higher the intensity ratio, *i.e.* I_{727}/I_{735} and I_{1248}/I_{1235}, the more ordered the structure of PC can be expected. These ratios are summarized in Table 1 and deconvoluted spectra are presented in Fig. S5. According to the results of the deconvolution the highest Raman crystallinity of PC composites was obtained for adsorption bed PC/Ae/C. Both series indicate that the degree of crystallinity, orderliness of PC-based materials, increase in the order initial PC/0 < PC/C < PC/Si/C < PC/Ae/C.

It was recently shown that the ordered crystalline structure of PC formed after the evaporation of its solution in THF strongly interacts with the surface of carbon fibres through π–π interactions of phenyl rings.[34] It can be assumed that such interactions also occur during the adsorption of nitroaromatic substances on prepared substrates. The increase in the adsorption of trinitrotoluene (TNT) for successive PC/C–PC/Si/C–PC/Ae/C substrates (see Fig. 6) can be correlated with the increase in crystallinity of these substrates as per Raman measurements (see Table 1). Finally, it should be added that in the reviewed literature on PC composites, no reports were found regarding the impact of inorganic particles added to them on the crystallinity of the composites.

3.4. Low-temperature nitrogen adsorption

The textural features of the studied materials (Table 2) show clear differences depending on the material composition. The S_{BET} of the samples of cotton and PC/C is very low (below 1 $m^2\ g^{-1}$). After introducing additional components (Aerosil R972V or silica) to the prepared materials, the S_{BET} significantly increased. The highest S_{BET} of 72.9 $m^2\ g^{-1}$ is observed for the material containing silica (PC/Si/C).

Fig. S6 presents the N_2 adsorption–desorption isotherms, which according to the IUPAC classification,[35] are type IV isotherms differing in hysteresis loop shapes depending on the composition of the studied material. For the cotton and PC/C sample, the hysteresis loop is hardly visible. It is characteristic of the materials with negligible porosity. For the PC/Ae/C sample, the H3 hysteresis loop is observed. It is characteristic of materials containing mesopores and macropores not completely filled with adsorbate. The presence of Aerosil resulted in an increase of N_2 adsorption compared to the material without this component. For PC/Ae/C a bimodal pore size distribution is observed with the dominant population of mesopores and macropores with diameters in the range of 10–80 nm and 80–200 nm (Fig. S7). The presence of silica in PC/Si/C material resulted in the H2 hysteresis loop typical of porous adsorbents, *e.g.* inorganic oxide gels (Fig. S6). The dominant population of mesopores with diameters in the range of 2–20 nm (Fig. S7) is responsible for the increased volume of adsorbed nitrogen compared to the PC/C.

3.5. SEM analysis

At 200× magnification (Fig. 4), the surfaces of PC/THF and PC/Ae samples are smooth except for mechanical damage. The PC/Si sample shows quite evenly distributed silica

Table 2 Physicochemical properties of the studied materials

Sample	Description	S_{BET}[a] ($m^2\ g^{-1}$)	V_p[b] ($cm^3\ g^{-1}$)	d_{av}[c] (nm)
a	Cotton	0.7	<0.01	9.6
b	Cotton + polycarbonate	0.6	<0.01	13.0
c	Cotton + polycarbonate + Aerosil R972V	24.6	0.14	23.0
d	Cotton + polycarbonate + silica	72.9	0.12	6.6

[a] S_{BET} – specific surface area determined based on the BET adsorption model. [b] V_p – total pore volume determined based on the BJH adsorption model. [c] d_{av} – average pore diameter.

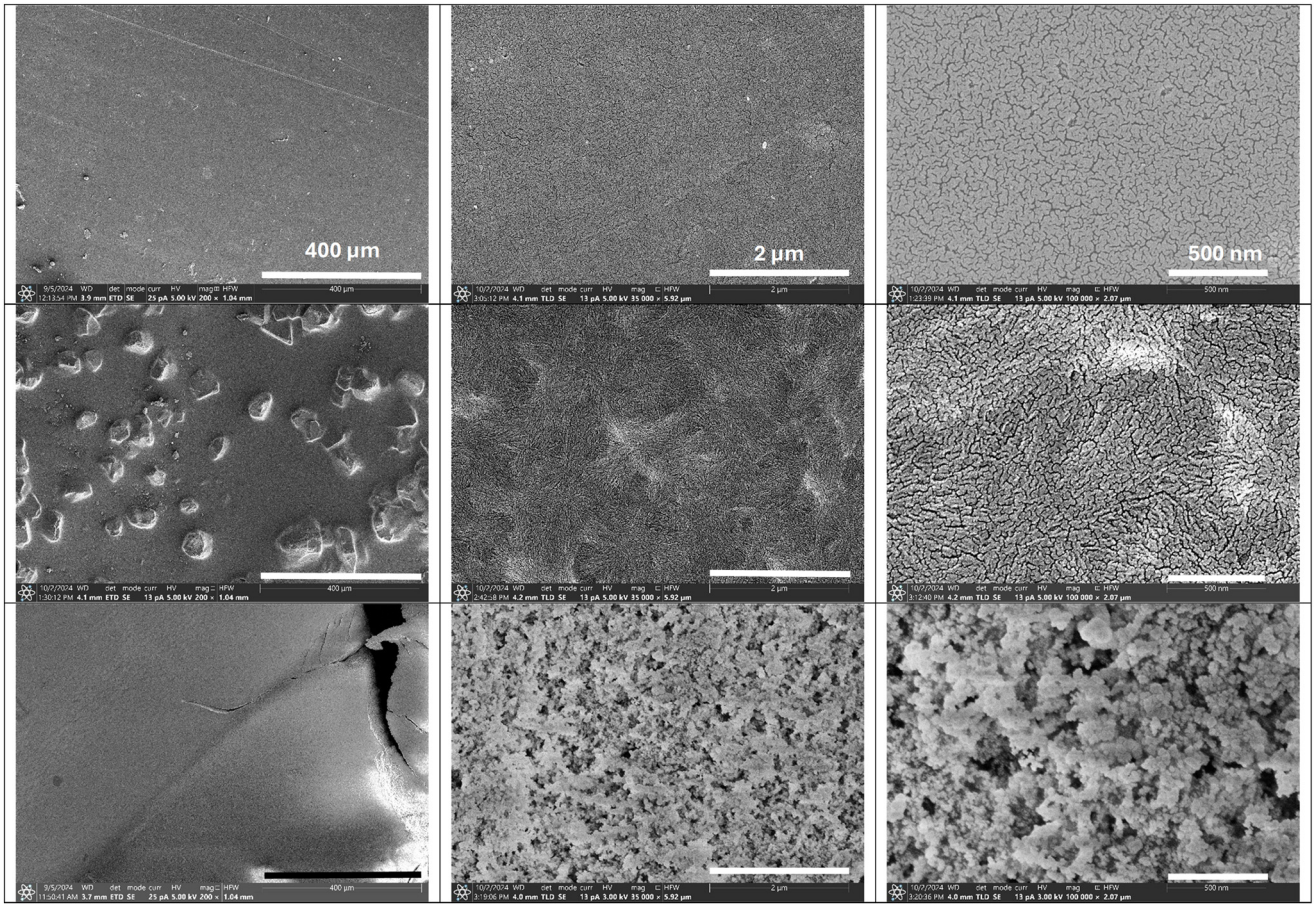

Fig. 4 SEM images of the prepared adsorbents. Top row, PC/THF; middle row, PC/silica; bottom row, PC/Aerosil. The columns represent different magnifications: left column 200×, central column 35 000×, and right column 100 000×.

particles surrounded by a smooth polycarbonate matrix. At a higher magnification of 35 000×, the PC/THF surface appears smooth, although some cracks can be observed at that stage. In contrast, the surface of the polymer in PC/Si changes; it is rough and irregular areas of different textures can be found. They appear as extended clusters of polymer phase of different densities or, alternatively, as structures grouped into bundles or cylinders.[36] At a corresponding magnification, the PC/Ae surface is uneven, with numerous holes, gaps and clusters of smaller, oval particles.

At an even higher magnification of 100 000×, narrow 50–100 nm long cracks can be observed on the smooth PC/THF surface. The PC/Si surface is more extensively cracked than the PC/THF, with many more, however wider cracks of similar length. At the highest magnification the PC/Ae surface is well developed and irregular, oval holes, pores measuring 50–200 nm, can be observed. Significantly smaller pores are also represented on the surface; however, it is difficult to determine their exact size based on SEM imaging. This is due to the blurred image induced by strong electrification of the Aerosil particles and their vibration. The porous structure of PC/Ae results from the granular structure of this composite. Large irregular particles of deposit formed by clumped smaller oval lumps can observed. The in-between formed pores provide channels for the penetration of water and nitroaromatic molecules into the surface layer and further penetration by capillary forces.

In SI section 5, scanning electron microscopy, the individual component images of Fig. 4 are presented separately as Fig. S8–S10.

3.6. Differential scanning calorimetry

The obtained DSC thermograms are summarized in Fig. 5. In the DSC curve recorded for the initial polycarbonate sample, the glass transition at 148 °C can be observed most clearly. It should be remembered that the investigated PC sample contains amorphous thermoplastic polycarbonate originating from molded sheets. The location of the transition and its effect are in agreement with literature data.[37] Two endothermic peaks with maximum at 143 °C and 208 °C were recorded on the DSC curve of the sample obtained by evaporating the PC solution in THF. They correspond to the PC melting process; the first one relates to the melting and crystallization of the polymer fraction crystallized from the solution,[38] while the second transition corresponds to the melting of the fraction formed by recrystallization of the molten fraction at a low-temperature transition, *i.e.* at 143

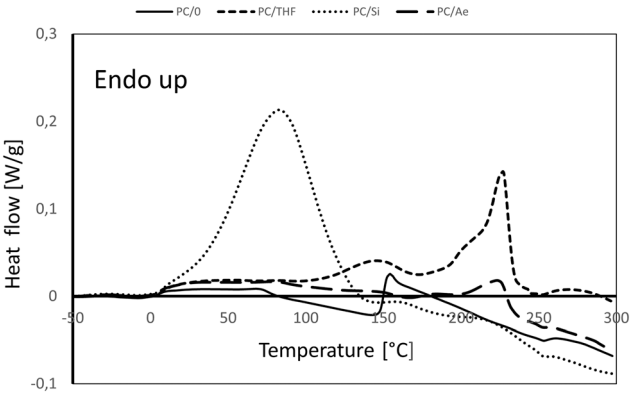

Fig. 5 DSC curve obtained for initial PC and prepared samples. Solid line, initial PC; dashed line, PC/THF; dotted line, PC/silica; and loosely dashed line, PC/Aerosil sample.

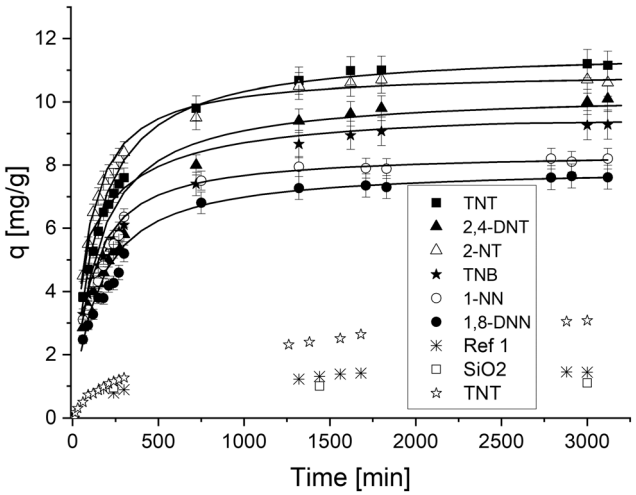

Fig. 6 Adsorption kinetics of nitroaromatic substances in laboratory scale – 1 L. Concentration of substances, 25 mg L^{-1} in water. For the assignment of symbols to shortcuts of six explosives see figure legend. These experiments were carried out on the PC/Ae/C bed. Data shown as scatter graphs represent: * TNT adsorption on PC/C adsorbent, □ TNT adsorption on bulk silica in water suspension (1.5 g L^{-1}), and ☆ TNT adsorption on PC/Si/C. Solid lines represent the non-linear model fitting of the PSO equation.

°C.[39] The enthalpy of the first process is significantly lower than the other one, as the endothermic melting process is superimposed with the exothermic crystallization process. In the DSC curves for PC/Si and PC/Ae, the melting effects of polycarbonate are not as pronounced as in the THF-evaporated sample. In the PC/Si curve, quite small endothermic transitions at 160 °C and 218 °C can be observed, while a clear transition is seen for the PC/Ae sample at 223 °C. The large endothermic peak visible for PC/Si in the 0–140 °C range and the maximum at 75 °C reflects the evaporation of water from the silica pores.

The above discussion of thermograms leads to concluding on the low content of crystalline phase formed in PC/Si and PC/Ae samples after THF evaporation. The presence of solid filler hinders the initial crystallization of PC. The sample recrystallizes only after heating (*vide supra*), whilst a melting process is observed at higher temperatures. This process is observable only for the PC/Ae sample. The more effortless recrystallization of this sample can be explained primarily by the nanometric particle size of Aerosil, *i.e.* an average primary particle size of 16 nm, which does not interfere with the formation of crystal lamellae such as crystalline nanofibers.

3.7. Adsorption on beds

3.7.1. Laboratory scale – 1 L. The experimental setup was established for TNT and then repeated for other nitroaromatics. First, the mixing intensity was determined. It was observed that the system utilizing a mixing rate of 200 rpm involved floating of all the pieces of the bed in the mixed phase. With an increased mixing rate, gradually the solution became cloudy, indicating separation of the bed from the cotton surface. Subsequent experiments were conducted to determine if desalting the solution affected the rate of removal of TNT from the solution. For both 1 wt% and 5 wt% NaCl, no increase in TNT adsorption on the bed was observed. Higher NaCl concentrations were not used in the starting solutions due to the noticeable drop in TNT concentration, probably due to its precipitation (unpublished data). Hence, further experiments were performed at 200 rpm without using the desalting process.

Fig. 6 shows the TNT adsorption run for up to 50 hours on the PC/Ae/C and PC/Si/C bed. The same figure also shows the adsorption of TNT on a bed containing only PC as well as adsorption concentration change over time for a TNT solution where 1.5 g of silica was added. No experiment was performed for hydrophobic Aerosil, which could not be dispersed in water. The comparison leads to the first conclusion, *i.e.* poor adsorption of TNT on the PC/C bed and a tiny loss of TNT for the silica suspension. Fig. 6 can be used to estimate that these effects constitute about 10% of the adsorbed amount of TNT observed for the PC/Ae/C bed. Furthermore, it can be observed that the adsorbed amount of TNT on the PC/Si/C bed is significantly lower than in the case of the PC/Ae/C bed. For example, after 24 hours of experiment, the amount of adsorbed TNT was about 3 mg g^{-1}, while for PC/Ae/C it was over 12 mg g^{-1}. Therefore, only the PC/Ae/C bed was used further in adsorption studies.

Fig. 6 also includes the results for other substances. The curves depicted therein represent the non-linear model fitting of the PSO equation using the obtained k_2 and q_e values (Table 3).

The analysis of the curves leads to the conclusion that an adsorption equilibrium state is reached for all analytes after 24 hours of running the process. The highest adsorbed amount was obtained at this point for TNT and 2-NT, whereas the lowest one was for nitronaphthalenes. At the initial stage, the curve's run shows that the most rapid increase in adsorption is observed for 2-NT and TNT, whereas the poorest increase is for 1,8-DNT. In consideration of the variations in the concentrations of explosives in solutions

Table 3 Kinetic parameters for adsorption of nitroaromatics on PC/Ae/C. Experiments in the laboratory scale (1 L) and bench scale (16 L)

		Pseudo-first-order			Pseudo-second-order			River water 48 h
Substance	q (mg g^{-1})	q_e (mg g^{-1})	k_1 (1 min^{-1})	R^2	q_e (mg g^{-1})	k_2 (g mg^{-1} min^{-1})	R^2	q_{river} (mg g^{-1})
Laboratory scale 1 L								
2,4,6-TNT	11.20	7.67	0.00193	0.962	11.65	0.00067	0.999	12.10
2,4-DNT	10.10	8.08	0.00180	0.959	10.30	0.00076	0.997	10.80
2-NT	10.66	5.16	0.00174	0.908	10.96	0.00116	0.999	9.85
1,3,5-TNB	9.49	7.16	0.00184	0.979	9.81	0.00073	0.998	8.30
1-NN	8.20	4.95	0.00182	0.929	8.41	0.00123	0.999	9.10
1,8-DNN	7.65	5.33	0.00174	0.956	7.94	0.00092	0.998	8.05
Bench scale 16 L								
2,4,6-TNT	9.15	7.83	0.00342	0.958	10.06	0.00063	0.999	
2,4-DNT	8.36	7.36	0.00351	0.960	9.20	0.00066	0.997	
2-NT	8.80	4.05	0.00358	0.857	9.05	0.00176	0.999	
1,3,5-TNB	8.16	7.08	0.00303	0.964	8.91	0.00065	0.997	

q – experimental equilibrium adsorption. q_e – calculated equilibrium adsorption. k_1 – rate constant of the PFO kinetic equation. k_2 – rate constant of the PSO kinetic equation. R^2 – coefficient of determination. q_{river} – experimental equilibrium adsorption for river water.

during the 1 L scale experiments, it was determined that by using the PC/Ae/C bed, 94% TNT, 89% 2-NT and nearly 75% 2,4-DNT were removed from solution. In the case of nitrotoluenes, approximately 60% of the amount was removed.

Based on the R^2 values summarized in Table 3, it is evident that the adsorption process of nitroaromatics on the PC/Ae/C bed is less consistent with the pseudo-first-order (PFO) kinetic model compared to the pseudo-second-order (PSO) model. In the case of the PSO equation, R^2 values exceed 0.99 for all compounds. Fig. S12 in the SI presents the fittings of the applied kinetic models in the form of linear equations to the obtained experimental data. For the PSO model, an excellent fit of the data to the linear equation can be observed, which is consistent with the high R^2 values. Good fitting to the PSO kinetic model suggests that in addition to the diffusion of nitroaromatic molecules to the surface of the sorbent bed, the adsorption rate may also be influenced by intraparticle diffusion as well as the occurrence of π–π interactions between the π-acceptor (nitroaromatics) and the π-donor (polycarbonate surface). For such interactions to occur, a proper spatial orientation of the donor and acceptor molecules is required.[40] A comparison of determined q_e equilibrium adsorption values and experimentally determined q values (Table 3) shows that q_e values calculated from the PSO equation are comparable with experimental equilibrium data. The maximum difference between q_e and q is 0.45 mg g^{-1}.

As shown in Table 3, the k_1 values obtained from the PFO model are relatively consistent (0.017–0.019 min^{-1}), whereas the k_2 values derived from the PSO model differ considerably (0.00067–0.00123 g mg^{-1} min^{-1}). These discrepancies in k_2 appear to correlate with the molecular structure of the adsorbates. The highest k_2 values were observed for nitro compounds containing a single nitro group (2-NT and 1-NN), while the lowest values were recorded for compounds with three nitro groups (2,4,6-TNT and 1,3,5-TNB). This suggests that the k_2 constant, which reflects the rate of adsorption (*i.e.*, the binding or settling of adsorbate molecules onto the adsorbent surface), may in this case be influenced by the molecular geometry and the accessibility of adsorption sites, potentially governed by π–π interactions (*vide supra*).

3.7.2. Laboratory scale – adsorption isotherms. The results presented in Table 4 summarize the constants calculated from the linearized forms of the Langmuir and Freundlich models as well as the corresponding R^2 values. Higher R^2 values were obtained for the Freundlich model. Fig. 7 presents the experimental adsorption data obtained at the aforementioned three temperatures, along with curves representing the nonlinear Langmuir and Freundlich isotherm models,[31] plotted using the calculated constants Q_m and K_L as well as n and K_F. As can be seen in Fig. 8,

Table 4 Adsorption of TNT on the PC/Ae/C bed. Parameters for Langmuir and Freundlich isotherm models

Langmuir model			Freundlich model		
26 °C/299 K					
q_m (mg g^{-1})	K_L (L mg^{-1})	R^2	n	K_F (mg g^{-1} L$^{1/n}$ g$^{-1/n}$)	R^2
3.08 ± 0.21	5.05 ± 0.22	0.97	1.54 ± 0.15	3.98 ± 0.12	0.99
36 °C/309 K					
3.37 ± 0.19	2.97 ± 0.20	0.98	1.49 ± 0.18	3.14 ± 0.16	0.99
46 °C/319 K					
3.21 ± 0.18	1.94 ± 0.11	0.98	1.43 ± 0.14	2.36 ± 0.15	0.99

q_m – maximum adsorption capacity. K_L – Langmuir constant.n – constant. K_F – Freundlich constant. R^2 – coefficient of determination.

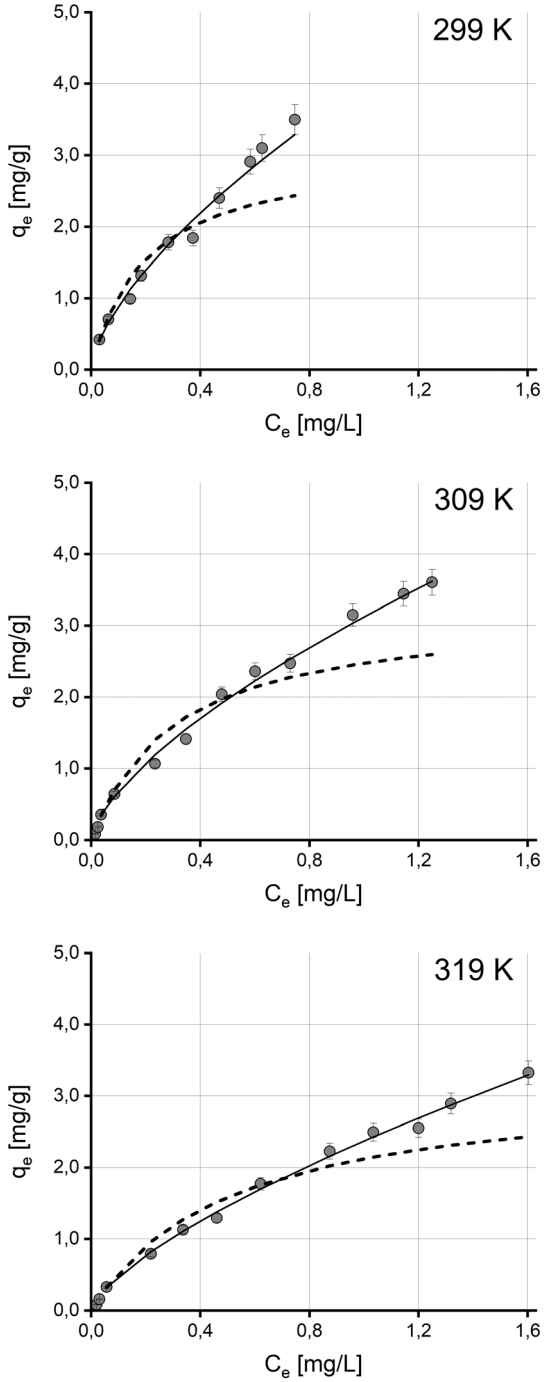

Fig. 7 Adsorption of TNT on PC/Ae/C bed at different temperatures (299 K, 309 K, 319 K) – grey circles. solid line – Freundlich non-linear model fit, dashed line – Langmuir non-linear model fit.

the curves representing the Freundlich isotherms show a very good fit to the experimental data over the entire range of equilibrium concentrations, while the Langmuir isotherms show only an acceptable fit at low concentrations. Therefore, it can be concluded that TNT adsorption in the studied system follows the Freundlich model and is based on multilayer adsorption on a heterogeneous surface.

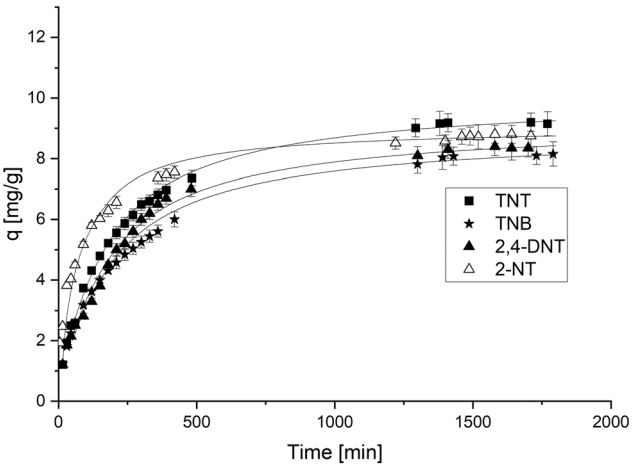

Fig. 8 Adsorption kinetics of nitroaromatic substances in bench scale – 16 L. Concentration of substances 25 mg L^{-1} in water. For the assignment of symbols to shortcuts of four explosives see figure legend. These experiments were carried out on PC/Ae/C adsorbent. Solid lines represent the non-linear model fitting of the PSO equation.

3.7.3. Laboratory scale – adsorption thermodynamics. The ΔG values presented in Table 5 are negative at all investigated temperatures, confirming that the adsorption of TNT onto the PC/Ae/C is spontaneous and thermodynamically favourable. The observed negative ΔH values indicate that the process is exothermic, with its intensity decreasing as the temperature increases. The ΔH values are greater than −40 kJ mol^{-1}, suggesting a physisorption mechanism.[41] The negative ΔS values indicate decreased randomness at the solid–liquid interface, likely resulting from the ordered adsorption of TNT on sorption sites *via* π–donor (*e.g.*, carbonyl groups or oxygen atoms in the C–O–C bonds of polycarbonate) to π–acceptor (electron-deficient aromatic ring of TNT) interactions. Furthermore, data from Table 5 suggest that the entropic contribution to the Gibbs free energy change is minimal, increasing it by approximately 4 kJ mol^{-1}. Therefore, TNT adsorption onto the PC/Ae/C composite is enthalpy-driven, involving relatively strong interactions with the surface. In conclusion, it is worth mentioning that the use of incorrect K_{eq} values in eqn (6) and (7) may, for example, lead to inconsistencies in the calculated values of ΔS.[42] Table 5 presents the value of ΔS calculated based on K_L expressed in L mg^{-1}. This value is over ten times lower than the correctly calculated ΔS based on the dimensionless constant K_L^0.

3.7.4. Laboratory scale – real surface water. The last column of Table 3 represents the collation of q_{river} adsorption values of nitroaromatic substances in the river water, obtained in experimental 1 L scale setup. It can be seen that q and q_{river} values are quite similar, and the differences between them are random, ranging from −1.19 to 0.90 mg g^{-1}. To determine whether the type of water affects the adsorption capacity on the PC/Ae/C bed, the average adsorption value was calculated from the results for six tested substances for each type of water. Then, using the *t*-test,[50] it was examined whether these average values differ statistically

Table 5 Thermodynamic parameters of TNT adsorption on the PC/Ae/C bed calculated based on the Langmuir equilibrium constant K_L and the dimensionless Langmuir equilibrium constant

Temperature [K]	K_L^0 [–]	K_L [L mg^{-1}]	ΔH [kJ mol^{-1}]	ΔS [J mol^{-1} K^{-1}]	$\Delta G°$ [kJ mol^{-1}]
299	1147306.54		−38.02	−11.17	−34.71
309	674326.26				−34.50
319	440632.20				−34.49
299		5.05	−38.02	−113.72	−4.03
309		2.97			−2.80
319		1.94			−1.76

ΔH – enthalpy change. ΔS – entropy change. $\Delta G°$ – Gibbs free energy change.

from each other. The test showed that there are no statistically significant differences at the 0.05 significance level between the obtained results – the mean experimental equilibrium adsorption values for nitroaromatics in river water and redistilled water. The calculated t value for data from Table 3 is $|t| = 0.176$. At a significance level of 0.05 and 10 degrees of freedom (6 + 6 − 2) the critical value is $t = 2.228$. The calculated t is less than the critical t value so the null hypothesis is retained: there is no evidence that the average equilibrium adsorption values for nitroaromatics in river water and redistilled water differ from each other. In conclusion, it can be assumed that the PC/Ae/C adsorbent is suitable for removing explosive substances from the real water sample, as used in the experiment. Most likely, river water dissolved components are not adequately adsorbed on the PC/Ae/C surface.

To confirm this hypothesis, primarily concerning dissolved organic matter (DOM), measurements were carried out using UV-vis spectroscopy in the range of 200–800 nm. UV-vis absorption is commonly used to provide information on DOM in aqueous systems.[51] The study was conducted on the original river water sample, on the same water after an experiment in a 1-liter scale with the PC/Ae/C composite (mass of the adsorptive phase *ca.* 36 g, see section 2, Materials and methods), and on the water after a 1-liter scale experiment using Norit SX-2 activated carbon (mass of the adsorbent 36 g). The results presented in Fig. S11 (SI) show that the UV spectra of the original sample and the sample after adsorption on the PC/Ae/C are nearly identical. It can only be concluded that absorbance in the 230–280 nm range is slightly reduced. In contrast, after adsorption on the activated carbon, a significant decrease in absorbance within this range was observed. Therefore, the conclusion regarding the weak adsorption of DOM on the PC/Ae/C composite seems to be confirmed. Strong adsorption of DOM on activated carbons has been reported in numerous studies.[52,53] The adsorption of soluble natural components causes a serious problem when using activated carbons to remove harmful pharmaceutical ingredients,[54] perfluorinated compounds,[55] or methylene blue dye[55] from surface water.

3.7.5. Bench scale – 16 L. Fig. 8 presents the results of kinetic experiments conducted at a 16 L scale for four nitroaromatic compounds. Similar to Fig. 6, which shows data for the 1 L scale, the curves represent a non-linear fit of the PSO model to the experimental data. Analysis of Fig. 8 indicates that the adsorption equilibrium state is reached for all analytes after 24–28 hours of process operation. The highest adsorbed amounts at this stage of the experiment were observed for TNT and 2-NT, while the lowest was recorded for TNB. At the initial stage of the process, the shape of the curves suggests that the most rapid increase in adsorption occurs for 2-NT, whereas the slowest increase is observed for TNB.

The lower part of Table 3 summarizes the parameter values calculated for the applied kinetic models, PFO and PSO, for the bench-scale. The linear fits of these kinetic models to the experimental data are shown in Fig. S13 in the SI.

Based on the highest R^2 values and the excellent agreement of the fitted lines with the experimental data, it is evident that the adsorption process of nitroaromatics at the 16 L scale, similarly to the 1 L scale, follows the PSO kinetic model. The good fit to the PSO model indicates that the adsorption process at both scales proceeds similarly, despite the completely different experimental setups, *i.e.* hydrodynamic conditions and mass transfer mechanism. Thus, in the 16 L setup, the nitroaromatic solution circulated through a glass column containing loosely packed, stationary bed fragments (1 × 1 cm), whereas in the 1 L setup, solution and bed mixing was carried out using a mechanical stirrer.

The adsorbent mass in the 16 L system was proportionally scaled up, *i.e.* sixteen times greater, while the analytes concentration remained the same (25 mg L^{-1}). The q_e values for the larger scale were approximately 0.9 to 1.9 mg g^{-1} lower, but overall, they can be considered comparable to those obtained at the 1 L scale. As observed for the 1 L scale, in the 16 L setup, the highest k_2 values was recorded for nitro compound containing one nitro group (2-NT), whereas the lowest k_2 values were obtained for compounds with three nitro groups in their molecules, namely TNT and TNB.

3.7.6. Solvent desorption studies. Cost-effectiveness analysis of the process in an industrial context. The possibility of desorbing TNT adsorbed on the PC/Ae/C bed was investigated during experiments conducted using acetonitrile (ACN). Using acetonitrile under the conditions described above, it was possible to wash out 64% (±12%) of the substance. It is worth mentioning that this experiment

Table 6 Examples of sorption capacities obtained for TNT on different adsorbents

Adsorbent	Method	C_0 TNT [mg L^{-1}]	TNT sorption capacity [mg g^{-1}]	Calculation method	Year/ref.
PC/Ae/C	KE	1–25	12	q_e from PSO kinetic model	This work
GAC	CDA	30–170	80	Breakthrough curves	2005/56
AC	BSE	10–100	10	Langmuir isotherm	2007/57
PAM/SiO_2	CDA	100	0.9	Breakthrough curves	2009/58
PTIM	BSE	50–350	400	Langmuir isotherm	2024/59
Clip-SOF	d-SPE	1	40	C_0 and C_R	2024/60
MWCNTs	BSE	100–400	40 (3-NT)	Langmuir isotherm	2009/61

C_0 – initial concentration of TNT. C_R – residual concentration TNT. PC/Ae/C – composite of polycarbonate and Aerosil on cotton. KE – kinetic experiments. GAC – granular activated carbon. AC – activated carbon. CDA – column dynamic adsorption. BSE – batch sorption experiments – shaking. PAM/SiO_2 – polyacrylamide grafted to SiO_2. PTIM – indole-based porous organic polymer. clip-SOF – glycoluril-derived molecular-clip-based supramolecular organic framework. d-SPE – dispersive solid phase extraction. MWCNTs – multiwalled carbon nanotubes. 3-NT – 3-nitrotoluene.

was performed using ACN under preliminarily selected, non-optimized conditions and was carried out solely to assess the efficiency of the desorption.

For the synthesized PC/Ae/C adsorbent, the material cost is primarily associated with Aerosil, priced at approximately €5 per kilogram. The other constituents, cotton, polycarbonate, and tetrahydrofuran, are waste-derived materials, for which market valuation is either negligible or indeterminate, especially since both waste collection and disposal incur costs.

According to the procedure detailed in the experimental section, the incorporation of 1 kg of Aerosil yields approximately 5 m^2 of adsorbent bed. In the desorption method outlined in the current section, ACN was utilized at a volume of 1 mL per cm^2 of adsorbent surface area. Accordingly, the desorption of a 5 m^2 bed would require 50 L of ACN. The cost of 1 L technical-grade ACN in the domestic market is approximately €10, resulting in a total solvent cost of €500. In comparison, the use of technical-grade acetone would reduce the total cost to approximately €100. Nevertheless, from a purely economic standpoint, solvent-based desorption remains financially unjustifiable.

The authors propose that the most economically viable and environmentally responsible method for the disposal of the used adsorbent beds is incineration. The presence of energetic compounds in a finely dispersed and phlegmatized form significantly mitigates the risk of detonation. Moreover, the explosives content in the deposit is at the level of 10 mg per gram (1% by weight), therefore a self-sustaining combustion reaction cannot occur.[43] It is also noteworthy that cotton- or cellulose-based medical wastes are commonly disposed of *via* incineration, providing an established precedent for this approach.

3.7.7. Estimation of the carbon footprint (GWP) for the PC/Ae/C adsorbent. The reported average carbon footprints (GWP) for the materials used are as follows: cotton 1 kg CO_2-eq. per kg,[44] polycarbonate 5 kg CO_2-eq. per kg,[45] and Aerosil average 1 kg CO_2-eq. per kg.[46] The average GWP of the prepared composite (produced from new, non-recycled materials) is 2.4 kg CO_2-eq. per kg. This was calculated based on the composition of the sorbent described in the paper: 35 wt% polycarbonate, 35 wt% Aerosil, and 30 wt% cotton. It should be noted, however, that extending the lifespan of products and promoting their reuse can significantly reduce their carbon footprint. For instance, for PET (a polymer containing chemical groups similar to those in polycarbonate), recycling can reduce the GWP by a factor of four,[47] while for cotton, the reduction can reach 25%.[48] The data for PET was used because no data for recycled polycarbonate could be found. Calculations based on these reductions yield an average GWP of approximately 1.0 kg CO_2-eq. per kg for the prepared adsorbent.

When comparing the sorption capacities for TNT on the adsorbents listed in Table 6, it becomes evident that granular activated carbon (GAC) has a capacity about seven times higher than that of the PC/Ae/C sorbent. Therefore, assuming that seven times more of the PC/Ae/C composite would be required to achieve the same TNT removal efficiency, the total GWP for 7 kg of this sorbent would amount to 7 kg CO_2-eq. (recycled components) and 16 kg CO_2-eq. (non-recycled components). At the same time the mean GWP reported in the literature for GAC is 11 kg CO_2-eq. per kg.[49]

Taking into account the energy and chemicals required for the production and regeneration of GAC, the PC/Ae/C sorbent prepared from recycled components appears to have considerable potential, especially since it can be incinerated after use (section 3.7.4) with only a little mineral solid residue and provide energy for other processes in waste treatment plants.

4. Conclusions

The study demonstrated the effectiveness of a new material obtained in accordance with the principles of sustainable development and a circular economy for the removal of nitroaromatic explosives from water. The prepared material contained *ca.* 30% cotton, 35% polycarbonate and 35% fumed silica (Aerosil). While preparing the material, *i.e.* the fabric coated with adsorbent, the minimum environmental impact had to be ensured, *i.e.* (i) the material was obtained from waste cotton and polycarbonate raw materials, (ii) the used

silica and tetrahydrofuran (a waste solvent from chromatography) are environmentally harmless, (iii) the preparation process consumed little energy, it did not require the use of chemical reactions, (iv) the application of the prepared bed required the use of simple equipment and processing techniques, easily scalable to larger-scale processes.

The sorption capacities presented in this work for nitroaromatics (8–12 mg g^{-1}) are lower than those reported for more effective adsorbents, such as activated carbons, shown in Table 6. However, they can be regarded as promising results, especially when the significant drawbacks of other adsorbents are taken into account. For instance, the production of activated carbon, regardless of the precursor, requires chemicals, is energy-intensive and associated with significant emissions of gases such as CO_2, CO, H_2S, and hydrocarbons, while the synthesis of specialized polymers (Table 6) is time-consuming and often generates toxic waste. A major advantage of the obtained PC/Ae/C bed is usage of waste materials and also its relatively simple disposal through incineration, especially since, as previously shown, solvent desorption methods are economically unviable. The obtained results provide a foundation for further development of the proposed sorption material as well as the technology of application for the removal of harmful explosives from water. The expansion of the sorption column or the application of a series of smaller columns can be considered as well. In relation to the preparation process, primarily in terms of cost reduction and smaller environmental impact, Aerosil can be effectively replaced with other components such as natural aluminosilicates or recycled components such as fly ash.

Author contributions

Waldemar Tomaszewski: conceptualization, investigation (lab scale, FTIR, HPLC), formal analysis, writing – original draft, writing – review & editing. Andrzej Krasiński: conceptualization, investigation (bench scale), formal analysis, writing – review & editing. Magdalena Zybert: investigation (nitrogen adsorption). Piotr Wieciński: investigation (SEM). Tomasz Gołofit: investigation (DSC).

Conflicts of interest

The authors declare that they have no known competing financial interests or personal relationships that could have appeared to influence the work reported in this paper.

Data availability

All data are available in the main manuscript and SI.

Supplementary information is available: The SI includes photos of the raw materials used, as well as additional experimental results that further illustrate the findings presented in the main text. Specifically, they pertain to Raman analysis, nitrogen adsorption, scanning electron microscopy, UV-Vis spectrophotometry, and the fittings of adsorption kinetic models to the experimental data. See DOI: **https://doi.org/10.1039/D5EW00669D**.

Acknowledgements

The authors would like to thank Prof. Grażyna Zofia Żukowska for her help with the Raman analysis. This work was supported by Warsaw University of Technology (Politechnika Warszawska) under I-Chem.4 project of the Scientific Council for Chemical Engineering.

References

1 Materials Market Report 2023 - Textile Exchange, **https://textileexchange.org/knowledge-center/reports/materials-market-report-2023/**, (accessed 21 October 2024).
2 Plastics Europe launches Plastics – the fast Facts 2023 · Plastics Europe, **https://plasticseurope.org/media/plastics-europe-launches-the-plastics-the-fast-facts-2023/**, (accessed 21 October 2024).
3 M. Tripathi, M. Sharma, S. Bala, V. K. Thakur, A. Singh, K. Dashora, P. Hart and V. K. Gupta, *Curr. Res. Biotechnol.*, 2024, **7**, 100225.
4 M. Y. Khalid, Z. U. Arif, W. Ahmed and H. Arshad, *Sustainable Mater. Technol.*, 2022, **31**, e00382.
5 R. M. Abdelhameed, M. El-Zawahry and H. E. Emam, *Polymer*, 2018, **155**, 225–234.
6 Y.-J. L. Mi-Kyung Kim, S.-H. Yoon and T.-K. Kim, *J. Korean Soc. Dye. Finish.*, 2005, **17**, 20–29.
7 D. Tian, X. Zhang, C. Lu, G. Yuan, W. Zhang and Z. Zhou, *Cellulose*, 2014, **21**, 473–484.
8 M. Mahmoud Nasef, H. Saidi, Z. Ujang and K. Z. Mohd Dahlan, *J. Chil. Chem. Soc.*, 2010, **55**, 421–427.
9 J. Saleem, M. Adil Riaz and M. Gordon, *J. Hazard. Mater.*, 2018, **341**, 424–437.
10 N. A. El Essawy, S. M. Ali, H. A. Farag, A. H. Konsowa, M. Elnouby and H. A. Hamad, *Ecotoxicol. Environ. Saf.*, 2017, **145**, 57–68.
11 B. Hoek, *Med. Confl. Surviv.*, 2004, **20**, 326–333.
12 J. C. Pennington and J. M. Brannon, *Thermochim. Acta*, 2002, **384**, 163–172.
13 R. A. Young, in *Encyclopedia of Toxicology*, Elsevier, 2014, pp. 179–182.
14 GUIDE TO EXPLOSIVE ORDNANCE POLLUTION OF THE ENVIRONMENT - GICHD, **https://www.gichd.org/publications-resources/publications/guide-to-explosive-ordnance-pollution-of-the-environment-1/**, (accessed 22 October 2024).
15 J. D. Rodgers and N. J. Bunce, *Water Res.*, 2001, **35**, 2101–2111.
16 S. Olavi Pehkonen, S. Zou, Y.-T. Hung, J. Paul Chen and L. Wang, in *Handbook of Industrial and Hazardous Wastes Treatment*, CRC Press, 2004, pp. 1113–1124.
17 G. Yardin and S. Chiron, *Chemosphere*, 2006, **62**, 1395–1402.
18 P. P. Kanekar, S. S. Sarnaik, P. S. Dautpure, V. P. Patil and S. P. Kanekar, 2014, pp. 67–86.

19 K. Panz and K. Miksch, *J. Environ. Manage.*, 2012, **113**, 85–92.
20 J. T. Walsh, R. C. Chalk and C. Merritt, *Anal. Chem.*, 1973, **45**, 1215–1220.
21 H. M. Heilmann, U. Wiesmann and M. K. Stenstrom, *Environ. Sci. Technol.*, 1996, **30**, 1485–1492.
22 P. C. Ho and C. S. Daw, *Environ. Sci. Technol.*, 1988, **22**, 919–924.
23 K. Misra, S. K. Kapoor and R. C. Bansal, *J. Environ. Monit.*, 2002, **4**, 462–464.
24 B. Charmas, M. Zięzio, W. Tomaszewski and K. Kucio, *Colloids Surf., A*, 2022, **645**, 128889.
25 G. L. McEneff, B. Murphy, T. Webb, D. Wood, R. Irlam, J. Mills, D. Green and L. P. Barron, *Sci. Rep.*, 2018, **8**, 5815.
26 W. Tomaszewski, V. M. Gun'ko and J. Skubiszewska-Zięba, *J. Sep. Sci.*, 2016, **39**, 1524–1532.
27 E. C. L. Mohammad Hadi Dehghani, S. Ahmadi, S. Ghosh, A. Othmani, C. Osagie, M. Meskini, S. S. AlKafaas, A. Malloum, W. A. Khanday, A. O. Jacob, Ö. Gökkuş, A. Oroke, O. M. Chineme and R. R. Karri, *Arabian J. Chem.*, 2023, **16**, 105303.
28 M. V. Galaburda, V. M. Bogatyrov, W. Tomaszewski, O. I. Oranska, M. V. Borysenko, J. Skubiszewska-Zięba and V. M. Gun'ko, *Colloids Surf., A*, 2017, **529**, 950–958.
29 G. Crini, H. N. Peindy, F. Gimbert and C. Robert, *Sep. Purif. Technol.*, 2007, **53**, 97–110.
30 Y. S. Ho and G. McKay, *Process Biochem.*, 1999, **34**, 451–465.
31 K. Y. Foo and B. H. Hameed, *Chem. Eng. J.*, 2010, **156**, 2–10.
32 P. S. Ghosal and A. K. Gupta, *J. Mol. Liq.*, 2017, **225**, 137–146.
33 J. Dybal, P. Schmidt, J. Baldrian and J. Kratochvíl, *Macromolecules*, 1998, **31**, 6611–6619.
34 H. Uematsu, N. Higashitani, A. Yamaguchi, A. Fukuishima, T. Asano, S. Mitsudo, S. Sugihara, M. Yamane, T. Irisawa, Y. Ozaki and S. Tanoue, *Surf. Interfaces*, 2022, **34**, 102300.
35 M. Thommes, K. Kaneko, A. V. Neimark, J. P. Olivier, F. Rodriguez-Reinoso, J. Rouquerol and K. S. W. Sing, *Pure Appl. Chem.*, 2015, **87**, 1051–1069.
36 Y. Xu, Y. Gao, X. Wang, J. Jiang, J. Hou and Q. Li, *Macromol. Mater. Eng.*, 2017, **302**, 1700054.
37 R. F. Boyer, *J. Macromol. Sci., Part B:Phys.*, 1973, **7**, 487–501.
38 H. Schorn, M. Heß and R. Kosfeld, in *Integration of Fundamental Polymer Science and Technology—2*, Springer Netherlands, Dordrecht, 1988, pp. 385–388.
39 S. Sohn, A. Alizadeh and H. Marand, *Polymer*, 2000, **41**, 8879–8886.
40 R. Thakuria, N. K. Nath and B. K. Saha, *Cryst. Growth Des.*, 2019, **19**, 523–528.
41 V. J. Inglezakis and A. A. Zorpas, *Desalin. Water Treat.*, 2012, **39**, 149–157.
42 H. N. Tran, *Adsorpt. Sci. Technol.*, 2022, 5553212.
43 The European Standard EN 1127-1:2007, Explosive atmospheres - Explosion prevention and protection - Part 1: Basic concepts and methodology, European Committee For Standardization 2007, Brussels.
44 S. S. Madhuri Nigam, P. Mandade and B. Chanana, *Int. Arch. Appl. Sci. Technol.*, 2016, **7**, 06–12.
45 Appendix B Eco - and supply-chain data, in *Materials and the Environment: Eco-informed Material Choice*, ed. M. Ashby, Butterworth-Heinemann an imprint of Elsevier, 3rd edn, 2021, pp. 403–429.
46 **https://hpqsilicon.com/wp-content/uploads/2024/08/HPQ_DECK_AUGUST_29_2024_V1.pdf**.
47 E. W. Gabisa, C. Ratanatamskul and S. H. Gheewala, *Sustainability*, 2023, **15**, 11529.
48 S. Roy, Y. Y. J. Chu and S. S. Chopra, *Resour. Conserv. Recycl. Adv.*, 2023, **19**, 200177.
49 P. Bayer, E. Heuer, U. Karl and M. Finkel, *Water Res.*, 2005, **39**, 1719–1728.
50 M. H. Herzog, G. Francis and A. Clarke, in *Understanding Statistics and Experimental Design. Learning Materials in Biosciences*, Springer, Cham, 2019, pp. 51–59.
51 E. C. Minor, M. M. Swenson, B. M. Mattson and A. R. Oyler, *Environ. Sci.:Processes Impacts*, 2014, **16**, 2064–2079.
52 T. Karanfil, M. Kitis, J. E. Kilduff and A. Wigton, *Environ. Sci. Technol.*, 1999, **33**, 3225–3233.
53 B. Schreiber, T. Brinkmann, V. Schmalz and E. Worch, *Water Res.*, 2005, **39**, 3449–3456.
54 L. F. Delgado, P. Charles, K. Glucina and C. Morlay, *Sep. Sci. Technol.*, 2015, **50**, 1487–1496.
55 J. Yu and J. Hu, *J. Environ. Eng.*, 2011, **137**, 945–951.
56 V. Marinović, M. Ristić and M. Dostanić, *J. Hazard. Mater.*, 2005, **117**, 121–128.
57 J.-W. Lee, T.-H. Yang, W.-G. Shim, T.-O. Kwon and I.-S. Moon, *J. Hazard. Mater.*, 2007, **141**, 185–192.
58 F. An, X. Feng and B. Gao, *J. Hazard. Mater.*, 2009, **168**, 352–357.
59 Y. Xu, H. Zhu, S. Mo, Y. Mao, C. Zhong, Y. Huang, R. Yuan, M. Zheng, M. Zhou and G. Chang, *Polymer*, 2024, **300**, 126993.
60 Y. Liu, S. Zeng, X. He, Y. Wu, Y. Liu and Y. Wang, *Molecules*, 2024, **29**, 5822.
61 X.-E. Shen, X.-Q. Shan, D.-M. Dong, X.-Y. Hua and G. Owens, *J. Colloid Interface Sci.*, 2009, **330**, 1–8.

